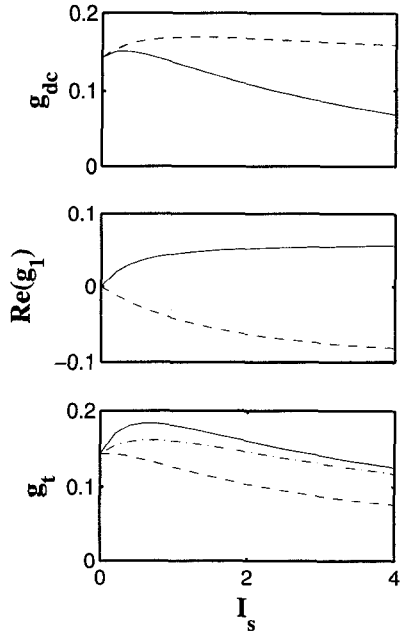


**CWB8 Fig. 1.** Dependence of the average gain coefficient ($g_{dc}$), the first Fourier coefficient ($g_1$), and the total gain ($g_t = g_{dc} + g_1$) for the case where the peaks of the signal interference pattern coincide with the intensity minima (solid curve) or maxima (dashed curve) of the pump interference pattern. For a comparison, the gain in the incoherent case where the signal waves do not interfere is also shown in (c) (dashdot curve). The intensities of the counterpropagating signal waves are assumed to be equal.

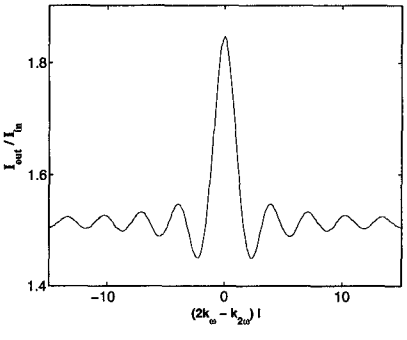


**CWB8 Fig. 2.** Reflectivity of three-level amplifier that is attached to an ideal mirror versus the detuning between the signal and the pump interference patterns ($\Delta kl \equiv 2k_s - k_p$, where $k_p$ and $k_s$ are the wave numbers of the signal and pump waves, and $l$ is the amplifier length).

The figure indicates that the sign of $Re\{g_1\}$, which determines whether the diffraction from the induced grating increases or decreases the total gain, is dependent on the relative phase between the interference patterns of the pump and the signal waves. The sign of $Re\{g_1\}$ is determined by the amplifier regions where the saturation effects are most effective. In the case where the periodic maxima of the signal interference pattern is located at the absorbing regions, $Re\{g_1\} > 0$, while $Re\{g_1\} < 0$ when it coincides with the amplifying regions. Changes in the wavelength or the optical phases of the counterpropagating signal waves significantly affect the signal gain. In order to analyze the filtering behavior of the effect, the reflectivity from a three-level optical amplifier that is attached to an ideal mirror was calculated (Fig. 2) by numerically integrating the coupled-wave equations. The filtering behavior is similar to that obtained by Horowitz *et al.*,[5] and therefore we believe that periodic pumping can be used for obtaining single-mode operation of lasers. Modes, which are enhanced by the wave mixing (with $Re\{g_1\} > 0$) will be promoted, while other modes with lower modal gain will be rejected. The lasing frequency can be controlled by changing the frequency and the phases of the pump waves unlike in Horowitz *et al.*[5] where the lasing frequency was self-determined.


1. R. Abrams, R. Lind, Opt. Lett. **2,** 94–96 (1978).
2. G.P. Agrawal, M. Lax, J. Opt. Soc. Am. **69,** 1717–1719 (1979).
3. B. Fischer, J.L. Zyskind, J.W. Sulhoff, D.J. DiGiovanni, Opt. Lett. **18,** 2108–2110 (1993).
4. S.J. Frisken, Opt. Lett. **17,** 1776–1778 (1992).
5. M. Horowitz, R. Daisy, B. Fischer, J. Zyskind, Opt. Lett. **19,** 1404–1406 (1994).
6. Y. Mitnick, M. Horowitz, B. Fischer, Bistability in cavities with erbium-doped fiber amplifier due to bidirectional pump-beam interference. To be published in J. Opt. Soc. Am. B (1997).


# CWC

**8:00 am–10:00 am**
Room 102

## Lasers for Telecom Applications

John E. Johnson, *Lucent Technologies/Bell Laboratories, Presider*

### CWC1 8:00 am

### Effect of many weak side modes on relative intensity noise of distributed feedback semiconductor lasers after dispersive propagation


Eva Peral, William K. Marshall,
Dan Provenzano, Amnon Yariv, *California Institute of Technology, MS 128-95, Pasadena, California 91125*


The performance of a lightwave communication system can be affected by the laser's relative intensity noise (RIN) and mode partition noise (MPN). In addition, measurements of RIN after propagation in fiber can be used to obtain several important intrinsic laser parameters. Therefore an accurate and simple model of RIN after dispersive propagation is necessary.

We report here an effect of MPN that can affect RIN in low-noise distributed feedback (DFB) lasers even with side-mode suppression ratios (SMSRs) higher than 40 dB and at frequencies up to 5 GHz, and which cannot be explained by previous single-mode models as in Marshall *et al.*[1]

We present a multimode theory of RIN after propagation in fiber in which the effect of FM to AM conversion in the fiber has been included via a generalization of the transfer function approach in Ref. 1 to the multimode case. The additional parameters that are needed in this multimode model are experimentally obtained from a measurement of the optical spectrum. This allows us to get theoretical fits that agree well with experimental measurements of RIN.

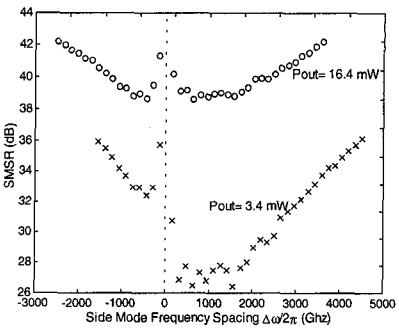


**CWC1 Fig. 1.** Side mode suppression ratio (SMSR) at Pout=3.4 mW (crosses) and Pout=16.4 mW (circles) as a function of the frequency deviation from the main mode.

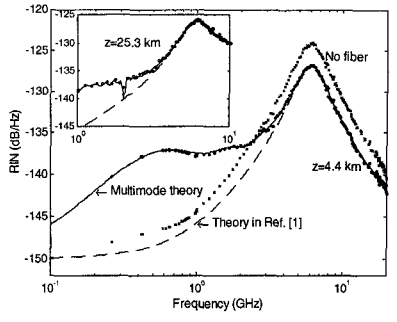


**CWC1 Fig. 2.** RIN measured before fiber and after 4.4 km and 25.3 km (inset) of fiber at Pout=3.4 mW, Ibias=1.6 Ith, SMSR=27 dB. The dots are experimental points after fiber, whereas crosses are before fiber. The solid line is the multimode theory and the dashed line is single-mode theory.

Since the gain spectrum in semiconductor lasers is broad, there usually exist many weak Fabry–Perot side modes that have similar optical power (see Fig. 1). These modes, while greatly suppressed relative to the main mode, together still can contribute enough power to affect the RIN after propagation in dispersive media such as optical fiber or fiber gratings. We find that even a multimode theory that includes a strong side mode does not necessarily predict what is experimentally observed.

The side modes are treated here as additive noise sources driving the carrier density and the photon density of the main mode. This simplification allows inclusion into the model of many side modes without much increase in computational cost.

We measured the RIN of a DFB laser before and after propagation in various lengths of standard single-mode optical fiber (Figs. 2 and 3). We also measured the optical spectrum (see Fig. 1) to determine the power in ~40 side modes, together with their separation from the

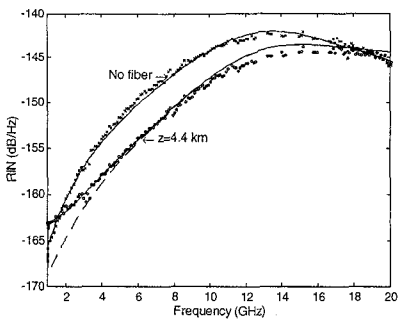


**CWC1 Fig. 3.** RIN measured after 4.4 km of fiber at Pout=16.4 mW, Ibias=4.1 Ith, SMSR=40 dB. The dots are experimental points after fiber, whereas crosses are before fiber. The solid line is the multimode theory and the dashed line is single-mode theory.

main mode. These data were input to our model, which satisfactorily explains the RIN measured.

Laser parameters were estimated from the RIN with and without fiber so as to obtain the best fits. For some fiber lengths the single-mode theory predicts a reduction in RIN,[1] which is not necessarily achieved experimentally due to these multimode effects. We have also observed a similar increase in RIN when a grating is used as optical filter.

1. W.K. Marshall, J. Paslaski, A. Yariv, Appl. Phys. Lett. **68,** 2496 (1996).

**CWC2** **8:15 am**

## Wavelength-addressable laser for reconfigurable WDM systems

Shan Zhong, Haifeng Li, Xiaohui Yang, Yung Jui Chen, D. Stone, *Department of Computer Science and Electrical Engineering, University of Maryland Baltimore County, and Joint Program for Advanced Electronic Materials, 1000 Hilltop Circle, Baltimore, Maryland 21250; E-mail: szhong1@engr.umbc.edu*

The applications of wavelength-addressable lasers in a wavelength division multiplexing (WDM) network have attracted much attention in recent years. A precision addressable laser source is particularly desirable for reconfigurable WDM network applications, such as a tunable transmitter for WDMA in local area networks (LANs) or reconfigurable add/drop multiplexers, in which a tunable laser source can replace an array of idling WDM lasers. The key requirement of this addressable laser is that it can be set to different wavelengths rapidly and accurately.

A multisection laser is an ideal candidate for such a laser source because it has the ability to have its output wavelength changed by varying the currents on different electrodes. Lasers of this type can be widely tunable, with ranges of up to 40 nm.[1] However the difficulty in implementing this type of device as an addressable source arises in obtaining the feedback information of lasing wavelength needed to accurately set or reset the controlling currents to achieve the desired wavelength.

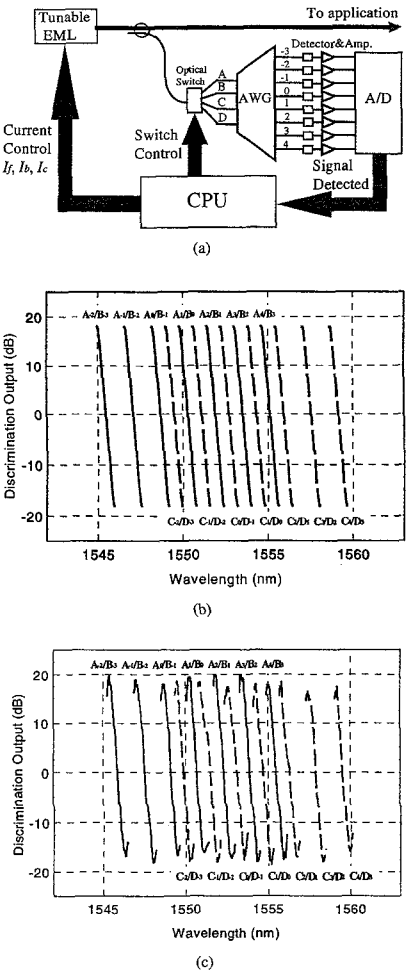


**CWC2 Fig. 1.** Schematic configuration of wavelength addressable laser. (a) Experiment setup. (b) Simulation results of a multichannel wavelength monitoring circuit. (c) Test results of a multichannel wavelength monitoring circuit.

A simple and efficient way to address this issue is to use a wavelength monitoring circuit to determine the output wavelength and use the feedback to control the current of each section for wavelength tuning.

Figure 1a shows the schematic diagram of our wavelength addressable laser setup. A small reference signal, tapped from the tunable laser, is sent to wavelength monitoring circuit, based on a specially designed 4 × 8 phased-array waveguide grating (PAWG).[4] We use one pair of inputs to monitor the laser wavelength. The logarithm ratio between the output throughputs of $A_j$ (A port input, output channel number j) and $B_{j-1}$ (B port input, output channel number j-1) has a linear characteristic with respect to the input wavelength (see Fig. 1b). Thus the precise wavelength can be readily determined by using this discrimination curve. Since each curve does not cover the full wavelength range of the channel spacing—the crosstalk figure of about −25dB to −30dB for our current PAWGs limits the useful range of the discrimination curves to 75% of the channel spacing or less—two pairs of input ports are used in our system to provide a complete coverage of the wavelength range. Figure 1c shows the measured discrimination curves for our PAWG device.

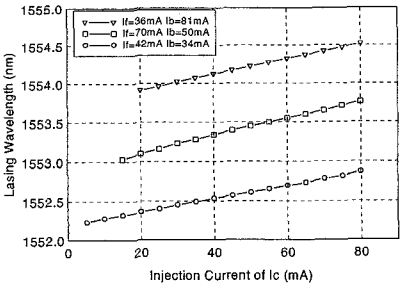


**CWC2 Fig. 2.** Characteristics of the tunable electroabsorption modulated laser integrated with a bent waveguide DFB laser.

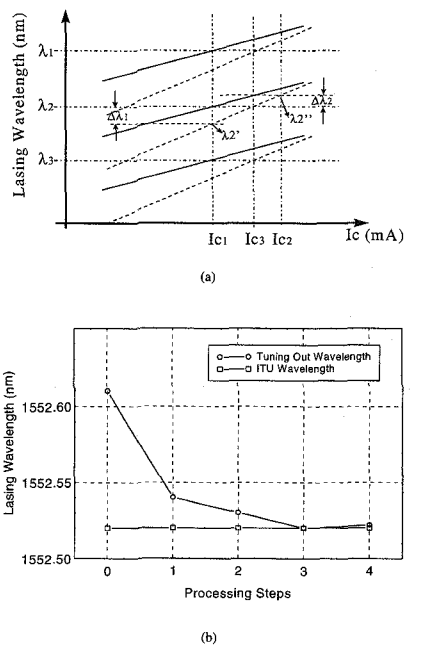


**CWC2 Fig. 3.** Wavelength tuning algorithm and experiment results. (a) Wavelength tuning algorithm. (b) The convergence of lasing wavelength to the desired value during the tuning steps.

The tunable laser used in this experiment is an electroabsorption modulated laser (EML) device integrated with a bent waveguide DFB laser,[3] with three current injection electrodes. Figure 2a shows the current conditions and tuning characteristics of the laser. The central electrode, $I_c$, is used to fine tune the lasing wavelength, while the two side electrodes ($I_b$ and $I_f$) are used to set the lasing wavelength to the International Telecommunications Union (ITU) wavelengths at the center of each tuning curve. A total tuning range of 2.7 nm was observed and wavelength tuning efficiency of $I_c$ is about 0.01 nm/mA.

To set the laser to an addressed ITU wavelength, $\lambda_2$, we first set the currents $I_f$ and $I_b$ to their corresponding biases and the current $I_c$ to the "best-guessed" value as determined by the calibration curves. The lasing wavelength, $\lambda_2'$, is then measured by the monitoring system. Based on the wavelength difference $\Delta\lambda_1 = \lambda_2 - \lambda_2'$, a modified current $I_c$ is determined and